Binding of Trivalent Arsenic Onto the Tetrahedral Au20 and Au19Pt Clusters: Implications in Adsorption and Sensing

ARTICLE *in* THE JOURNAL OF PHYSICAL CHEMISTRY A · JUNE 2015

Impact Factor: 2.69 · DOI: 10.1021/acs.jpca.5b03832

4 AUTHORS:

Diego Cortés-Arriagada

Pontifical Catholic University of Chile

15 PUBLICATIONS **56** CITATIONS

SEE PROFILE

María Paz Oyarzún Medina

University of Santiago, Chile

2 PUBLICATIONS **0** CITATIONS

SEE PROFILE

Luis Sanhueza

Universidad Austral de Chile

7 PUBLICATIONS **22** CITATIONS

SEE PROFILE

Alejandro Toro-Labbé

Pontifical Catholic University of Chile

223 PUBLICATIONS **4,349** CITATIONS

SEE PROFILE

THE JOURNAL OF PHYSICAL CHEMISTRY A

Article

pubs.acs.org/JPCA

Binding of Trivalent Arsenic onto the Tetrahedral Au_{20} and $Au_{19}Pt$ Clusters: Implications in Adsorption and Sensing

Diego Cortés-Arriagada,*[,†] María Paz Oyarzún,[‡] Luis Sanhueza,[§] and Alejandro Toro-Labbé[†]

[†]Nucleus Millennium Chemical Processes and Catalysis; Laboratorio de Química Teórica Computacional (QTC), Departamento de Química-Física, Facultad de Química, Pontificia Universidad Católica de Chile, Av. Vicuña Mackenna 4860, Macul, Santiago 9900087, Chile

[‡]Laboratorio de Electrocatálisis, Departamento de Química de los Materiales, Facultad de Química y Biología, Universidad de Santiago de Chile, Av. Libertador Bernardo O'Higgins 3363, Estación Central, Santiago 9170124, Chile

[§]Instituto de Ciencias Químicas, Facultad de Ciencias, Universidad Austral de Chile, Av. Las Encinas 220, Valdivia 5090000, Chile

Supporting Information

ABSTRACT: The interaction of arsenic(III) onto the tetrahedral Au_{20} cluster was studied computationally to get insights into the interaction of arsenic traces (presented in polluted waters) onto embedded electrodes with gold nanostructures. Pollutant interactions onto the vertex, edge, or inner gold atoms of Au_{20} were observed to have a covalent character by forming metal−arsenic or metal−oxygen bonding, with adsorption energies ranging from 0.5 to 0.8 eV, even with a stable physisorption; however, in aqueous media, the Au−vertex−pollutant interaction was found to be disadvantageous. The substituent effect of a platinum atom onto the Au_{20} cluster was evaluated to get insights into the changes in the adsorption and electronic properties of the adsorbent−adsorbate systems due to chemical doping. It was found that the dopant atom increases both the metal−pollutant adsorption energy and stability onto the support in a water media for all interaction modes; adsorption energies were found to be in a range of 0.6 to 1.8 eV. All interactions were determined to be accompanied by electron transfer as well as changes in the local reactivity that determine the amount of transferred charge and a decrease in the HOMO−LUMO energy gap with respect to the isolated substrate.

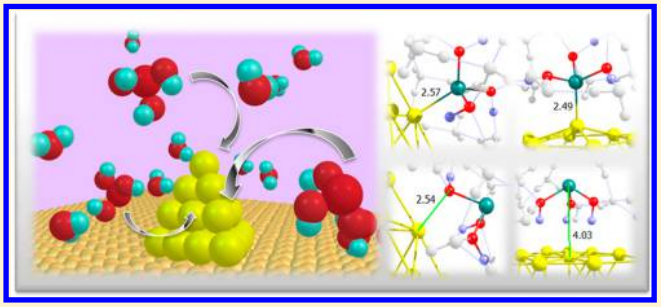

1. INTRODUCTION

Arsenic has been recognized as one of the world's greatest environmental hazards, threatening the lives of several hundred million people. The main sources of arsenic are both natural (by geochemical factors) and anthropogenic (through the use of insecticides, herbicides, phosphate fertilizers, mining and smelting, industrial processes, coal combustion, timber preservatives, among others).[1−3] In natural waters, arsenic exists as arsenite (the trivalent arsenic, As(III)), arsenate (the pentavalent arsenic, As(V)), monomethylarsonic acid (MMA), and dimethylarsinic acid (DMA).[4−6] It is important to note that the trivalent compounds are 60 times more toxic compared with those based on pentavalent arsenic;[7,8] in addition, the As (III) pollutants have a higher mobility from adsorbent surfaces,[7,8] which results in the low removal efficiencies. The constant exposure to contaminated drinking waters with high concentrations of arsenic (as established by the World Health Organization, >10 μg/L)[7,9] is associated with diseases such as atherosclerosis, hypertension, hyperkeratosis, chronic arsenicosis, and different forms of skin and lung cancers.[1,10] Because of these problems, the control of the arsenic levels in drinking waters is essential.

Experimental methods have been developed for the detection of arsenic traces in environmental matrixes, where the most widely used are chromatographic methods,[11,12] spectrophotometric,[13−15] and electrochemical techniques;[16−20] the latter has the advantage of having a low-cost instrumentation, fast analysis, and high sensitivity and selectivity. In this regard, the use of modified electrode surfaces have been extensively developed, with the use of nanomaterials, such as metal nanoparticles,[21−24] graphene,[10,25] and carbon nanotubes,[26−29] among others. In particular, gold nanoparticles incorporated onto electrode substrates have attracted extensive attention and bring a new area to the electrochemical determination of arsenic.[23,24,30−32] It has been reported that these modified electrodes can be considered as behaving as random arrays of microelectrodes, which provides advantages as the enhanced mass transfer, efficient catalysis, large surface area, and controllable microenvironment.[33]

Gold clusters have attracted considerable interest lately due to their potential technological applications.[34] Atomic quantum clusters are stable between 2 and 150 atoms, with average particle sizes in the range 0.5 to 2.0 nm. These very small particles exhibit unique properties through quantum size

Received: April 21, 2015
Revised: June 10, 2015

DOI: 10.1021/acs.jpca.5b03832
J. Phys. Chem. A XXXX, XXX, XXX−XXX

effects, which are dominant over classical Newtonian behavior, as a consequence of cluster sizes being comparable to electron Fermi wavelength.[35] Moreover, the atomic clusters have a high surface area and volume that allow a large number of binding sites available for catalysis or chemical sensing.[35,36] For instance, embedded small gold clusters onto transition-metal oxide supports have been determined to be good adsorbents and catalysts of small molecules such as CO, CO_2, and H_2.[37,38] In this line, the Au_{20} cluster is similar to a fragment of bulk face-centered cubic gold, which has a tetrahedral geometry, as determined from photoelectron spectroscopy and theoretical calculations,[39−42] suggesting the use of this cluster as a model of the bulk surface where each of the four faces of the tetrahedron represents an (111) surface. In addition, the vertex and edge atoms have different coordination environments and may also provide useful sites for adsorption, catalysis, and other applications.[37] Moreover, the Au_{20} cluster has been usefully used as a model of a gold nanostructure to study the oxidation of CO onto MgO/Mo(100) substrate embedded with Au nanoclusters.[43]

Taking into account the higher toxicity of arsenite, density functional theory (DFT) calculations are performed to understand the As(III) adsorption onto the Au_{20} and $Au_{19}Pt$ clusters, having as background the properties and interesting features of these systems. The bimetallic $Au_{19}Pt$ cluster was used as a model to evaluate the doping effects of Pt in the properties of the gold-based adsorbent. Moreover, this work will give us a theoretical basis whereby these systems would act and serve for the experimental adsorption and detection of As(III) through modified electrode surfaces with gold clusters, which would increase the response of the detection of this pollutant compared with other nanostructures.

2. COMPUTATIONAL DETAILS

At the DFT level, the PBE[44] functional was used in combination with the 6-31G(d,p)[45,46] basis set for H, O, and As; the quasirelativistic pseudopotential and basis set LANL2TZ[47−49] with extra f-polarization functions was adopted for Au and Pt as obtained from the EMSL basis set library.[50,51] We select the PBE functional because this performs well to reproduce properties of the Au dimer and Au_{20} cluster. (See the Supporting Information.) Furthermore, the reliability of the PBE functional is supported by recent studies.[52] The spin unrestricted formalism (UPBE) was used for calculations involving open-shell electronic states; mixture of higher spin states was found to be negligible. Dispersion force effects were included by the pairwise dispersion correction DFT-D3, in combination with the Becke−Johnson damping scheme to avoid repulsive interatomic forces at short distances.[53,54] Vibrational frequencies were computed to ensure that all of the molecular structures correspond to energy minima; that is, all of the ground states have only positive frequencies associated with all their vibrational modes. Atomic net charges and bonding characteristics were obtained from the natural bond orbital (NBO) analysis. Basis set superposition error (BSSE) were corrected by the counterpoise method.[55] All calculations were performed in the Gaussian 09 program.[56]

3. RESULTS AND DISCUSSION

The Au_{20} cluster is composed by three kind of Au atoms:[57] 4 vertex atoms (Au^v), 4 inner atoms (Au^i), and 12 edge atoms (Au^e). In accord with the T_d group, the electronic configuration of the tetrahedral Au_{20} cluster is $(t_2)^6(e)^4(t_2)^0$, and thus the HOMO is doubly degenerate and the LUMO is triply degenerate (Figure 1a). It is noted that the HOMO is mainly

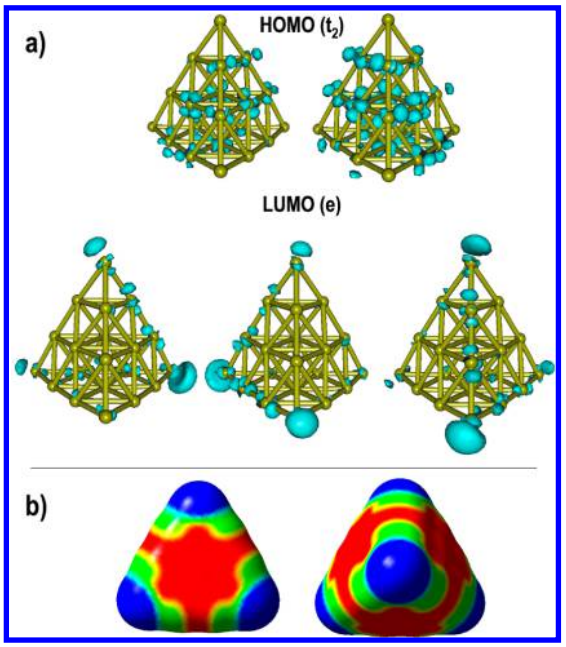

Figure 1. (a) HOMO (t_2) and LUMO (e) densities and (b) molecular electrostatic potential (MEP) of the tetrahedal Au_{20} cluster. In MEP, sites with negative and positive charge excesses are characterized by red and blue color, respectively.

due to s and d orbitals coming from the Au^e and Au^i atoms, respectively, which behave as electron donating for electrophiles. The LUMO is mainly due to the s orbitals of the Au^v atoms, which act as electron acceptors for nucleophiles. From the electrostatic framework, the molecular electrostatic potential (Figure 1b) shows as the Au^i atoms have a negative charge excesses (with a low contribution from the Au^e atoms), while the positive charge excesses are located in the Au^v atoms. Charges were computed to be $\sim +0.16|e|$ (Au^v), $\sim -0.18|e|$ (Au^i), and $\sim +0.01|e|$ (Au^e), in good agreement with previous reports.[57] The latter indicates that Au^v atoms are active sites for both charge-controlled and frontier-controlled interactions with the electron sufficient oxygen atoms in arsenite, and thus an electrostatic interaction with the negatively charged sites of the pollutant can allow the adsorption at the Au^v atoms for subsequent forming of an adduct by orbital interactions.

3.1. Adsorption of $As(OH)_3$ onto the Tetrahedral Au_{20} Cluster. In all calculations, we select the $As(OH)_3$ form of arsenite because this one is found to be dominant in neutral waters up to pH 9.2. Both arsenic and oxygen atoms were found as interacting sites for the Au^v, Au^i, and Au^e atoms (Figure 2). The adsorption strength was determined from the adsorption energy (E_{ads}) using the following expression: $E_{ads} = E(Au_{20}) + E(As(OH)_3) - E(Au_{20}{\cdot}As(OH)_3)$, where $E(Au_{20})$ and $E(As(OH)_3)$ are the total energies of the isolated Au_{20} and $As(OH)_3$ molecules, respectively, and $E(Au_{20}{\cdots}As(OH)_3)$ is the energy of the formed adduct. Positive values of E_{ads} indicate energetic stability for the $Au_{20}{\cdots}As(OH)_3$ systems.

The $Au_{20}{\cdots}As(OH)_3$ systems are depicted in Figure 2; the pollutant adsorption onto the Au^v, Au^e, and Au^i type atoms is analyzed, and the interaction energies are displayed in Table 1. Two stable conformations were obtained: (a) where the

DOI: 10.1021/acs.jpca.5b03832
J. Phys. Chem. A XXXX, XXX, XXX−XXX

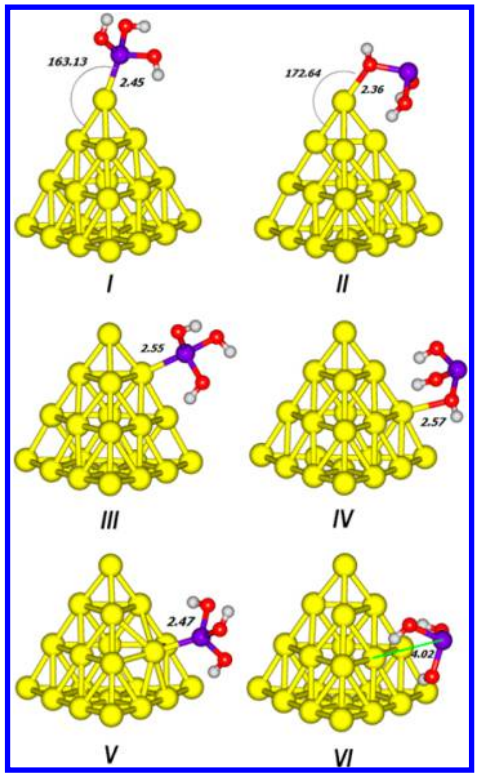

Figure 2. Molecular structures of the $Au_{20}\cdots As(OH)_3$ systems. Color code to atoms: white, hydrogen; red, oxygen; purple, arsenic; yellow, gold.

Table 1. Adsorption Energies in Electronvolts and Selected Atomic and Fragment Charges of the $Au_{20}\cdots As(OH)_3$ Systems

		charge of the adsorption site Au^x				
system	E_{ads}	before adsorption	after adsorption	ΔQ_{Au}	$Q_{As(OH)_3}$	Q_{As}
I	0.78	0.16	−0.10	−0.26	0.35	1.69[a]
II	0.61	0.16	0.19	0.03	0.20	1.59
III	0.69	0.01	−0.37	−0.38	0.41	1.75
IV	0.52	0.01	−0.07	−0.08	0.24	1.60
V	0.69	−0.18	−0.31	−0.13	0.51	1.79
VI	0.54	−0.18	−0.52	−0.34	0.23	1.60

[a]Charge of the arsenic atom in its isolated form is $Q_{As} = +1.53|e|$.

pollutant binds to the adsorbent by means of the arsenic atom (Au−As mode) and (b) where the pollutant binds to the adsorbent by means of the oxygen atom (Au−O mode). First, the pollutant interaction onto the Au^v type atom is displayed by structures **I** and **II**. The most stable conformation (**I**) is due to the Au−As mode, with an adsorption energy of 0.78 eV and bond lengths of d_{Au-As} = 2.45 Å, which is in the typical range for Au−As bonds of 2.44 to 2.46 Å.[58−60] The systems **II** shows the adsorption of $As(OH)_3$ onto the Au^v atom by the Au−O mode, with an adsorption energy of 0.61 eV, and the Au−O bond length is of d_{Au-O} = 2.36 Å, which is in agreement with the Au−O distances determined from theoretical calculations.[61] Note that two hydrogen atoms are directed toward an Au^e atom, suggesting an electrostatic interaction that enhances the stability for this conformation. The conformations **III** and **IV** are due to $As(OH)_3$ adsorption onto the Au^e atoms by means of the Au−As and Au−O mode, respectively; the adsorption energies in these cases are 0.69 (**III**) and 0.52 eV (**IV**). The bond lengths are increased compared with those obtained for adsorption in the Au^v atom, possibly by steric repulsion with the neighbor gold atoms. The Au−As and Au−O bond lengths reach values of d_{Au-As} = 2.55 and d_{Au-O} = 2.57 Å for systems **III** and **IV**, respectively, which is in agreement with a decrease in the adsorption strength. Finally, the $As(OH)_3$ adsorption onto the inner Au^i atom is depicted by systems **V** and **VI**, with adsorption energies of 0.69 and 0.54 eV, respectively. The Au−As bond length is of d_{Au-As} = 2.47 Å, and the Au^i atom expands out of the sideplane of the tetrahedral cluster by 0.9 Å, causing a decrease in the global stability of the system; however, both cases show an important contribution from dispersion forces with corrections to the adsorption energy of 0.39 and 0.41 eV for **V** and **VI** systems, respectively. Indeed, the $Au_{20}\cdots As(OH)_3$ interaction in the conformation **VI** appears entirely due to a noncovalent interaction, which is attributed to the high aromatic character of the Au_{20} cluster caused by the strong nuclear magnetic shielding in regions with deficient electron density;[41,57] in addition, stabilization by charge transfer is expected. Note that the pollutant adsorption in the Au^i atom was not obtained, possibly due to the high negative charge in the inner gold atom and oxygen that destabilizes the Au−O bonding. At first glance, we can see that different conformations for the $Au_{20}\cdots As(OH)_3$ systems can be obtained with reasonable adsorption energies, indicating the stability of a pollutant−substrate interaction.

The nature of the chemical binding for the metal-As and metal-O modes was analyzed in the framework of the NBO analysis. In those systems interacting in the Au−As mode (**I**, **III**, **V**), the Au−As bond has an σ covalent character, taking place between s- and sp-hybridized orbitals of the Au^v and arsenic atoms, respectively; besides, the Au^e atom develops sp hybridization for the Au−As bond. It is noted from the E_{ads} values that the covalent Au−As interaction is stronger than the Au−O bonding because the latter is a coordinate covalent bond. For instance, in the conformation **II**, an occupied oxygen lone pair (LP) (of p character) interacts with the low occupied LP of the Au^v atom (of s character), which acts as a Lewis acid. As the acceptor orbital is partially occupied, a low stability is expected compared with the Au−As covalent bond; indeed, a decrease in at least 0.1 eV in the stability is observed. In the system **IV**, the coordinate covalent bond appears to be less stable than that of conformation **II**, which is explained because the coordination of the oxygen LP is with an s (and p)-antibonding orbital (LP*) of the Au^e atom. Therefore, these results show that the $Au_{20}\cdots As(OH)_3$ system is mainly stabilized by interactions of chemical nature.

To account for the charge density distribution after the interaction, we analyze the atomic and fragment charges of the systems **I**−**VI** (Table 1). The charge in the pollutant ($Q_{As(OH)_3}$) is used as parameter for the electron transfer; a positive value of $Q_{As(OH)_3}$ indicates electron transfer toward the Au_{20} cluster. From Table 1, it is noted that an electron transfer toward the Au_{20} cluster occurs in all of the systems. The amount of charge transfer becomes to be higher for the systems involving an Au−As bond (with electron transfer of up to 0.51*e*) rather than those ones with an Au−O bond (with electron transfer of up to 0.24*e*). The latter agrees with the high stability of the Au−As mode compared with Au−O. It is worth noting that the results show that the Au−As mode appears to be stable in system **I**, even when the arsenic atom and the Au^v sites are positively charged in the isolated molecules. To clarify this statement, we

DOI: 10.1021/acs.jpca.5b03832
J. Phys. Chem. A XXXX, XXX, XXX−XXX

need to point out that the first step in the adsorption process is mainly a charge-controlled step that allows the diffusion of the pollutant (through the solvent) toward the adsorption sites;[62] in this case, the diffusion of the arsenic atom toward the Au^v atoms is clearly disadvantaged because both (the arsenic and Au^v atoms) are positively charged; however, if the arsenic atom in the $As(OH)_3$ molecule is close enough to the Au^v atom, inductive effects cause the adsorption site gain electron density from the arsenic atom, and the orbital interaction is allowed. Specifically, in the case of the system **I**, the pollutant transfers 0.35*e* toward Au_{20} cluster, of which 0.26e are localized in the adsorbent Au^v atom ($Q_{Au} = -0.10|e|$), while the arsenic has an increase in the positive charge ($Q_{As} = 1.69|e|$). Moreover, because of this difference in the atomic charges, the Au−As mode (systems **I**, **III**, and **V**) shows a polarized character with at least 75% of the bonding density polarized toward the positively charged arsenic atom. On the contrary, only up to 34% of the transferred electron density is retained by the adsorbent gold atom in systems **II** and **IV**, which is attributed to the characteristics of the As−O binding. For example, electron transfer of 0.24*e* takes place in the conformation **IV**, but the adsorbent Au^e atom changes its charge only in 0.08*e*, while the electron density is mainly delocalized in the surrounding gold atoms of the adsorbent site. Finally, it is noted that the physisorption strength in the system **VI** is stabilized by charge transfer of 0.23*e* toward the substrate. From these results, we can see that, in addition to chemical bonding, the $Au_{20}\cdots As(OH)_3$ system is stabilized by charge transfer toward the substrate, which is a good parameter to establish that the Au_{20} cluster serves to detection of arsenic(III) in its neutral form.

To get insights into the chemical phenomena dominating the charge transfer in the $Au_{20}\cdots As(OH)_3$ systems, we study the chemical reactivity descriptors associated with the electron transfer ability, such as the electronic chemical potential (μ) and electrophilicity (ω) (Table 2): μ characterizes the response

Table 2. Fragmental Reactivity indexes for $Au_{20}\cdots As(OH)_3$ Systems (in eV): Electronic Chemical Potential (μ_i) and Electrophilicity (ω_i)[a]

system	$\mu_{Au_{20}}$	$\mu_{As(OH)_3}$	$\Delta\mu$	$\omega_{Au_{20}}$	$\omega_{As(OH)_3}$	$\Delta\omega$
I	−4.95	−3.58	−1.37	14.58	2.47	12.11
II	−4.93	−3.95	−0.98	13.95	2.87	11.08
III	−4.93	−3.79	−1.13	14.06	2.77	11.29
IV	−4.92	−4.02	−0.90	13.89	2.89	11.01
V	−5.02	−3.76	−1.26	16.60	2.88	13.72
VI	−4.92	−3.99	−0.92	13.62	2.91	10.71
isolated	−4.92	−3.46	−1.46	13.62	2.13	11.48

[a] *i* stands for the fragment Au_{20} or $As(OH)_3$ in the adduct.

of the system energy with respect to changes in the electron number,[63] and thus is related to the electronegativity χ through $\mu = -\chi$; moreover, ω characterizes the electrophilic character, defined as the stability in energy that reaches the molecular system when it gains electrons.[63] Reactivity indexes were obtained as $\mu = (\varepsilon_{HOMO} + \varepsilon_{LUMO})/2$, $\omega = \mu^2/2\eta$, where η is the molecular hardness [defined as $\eta = (\varepsilon_{LUMO} - \varepsilon_{HOMO})/2$] and ε_{HOMO} and ε_{LUMO} are the eigenvalues of the HOMO and LUMO, respectively. To obtain the fragmental reactivity indexes for each fragment in the systems **I**−**VI**, we use the counterpoise method; that is, the wave function for fragment *i* is obtained considering its geometry and the complete basis set as in the adduct.

From Table 2, it is noted that in accord with the μ and ω indexes, the $As(OH)_3$ molecule behaves as a donor with respect to the Au_{20} cluster in its isolated state; the last one shows a high electrophilic character. Therefore, differences between the μ and ω indexes ($\Delta\mu = -1.46$ eV, $\Delta\omega = 11.48$ eV) suggest that electron transfer must occur in the $As(OH)_3 \rightarrow Au_{20}$ direction, as previously suggested from the electron population analysis. When pollutant binds to the substrate, the orbital interaction and the different interaction modes affect the HOMO−LUMO energy levels; therefore, different behaviors in the reactivity of the fragments are expected and determine the amount of transferred electrons. As previously noted, the largest charge transfer is reached in the Au−As mode, and reactivity descriptors gives insights into this fact. First, it is noted that the $\mu_{Au_{20}}$ value is slightly larger for systems in the Au−As mode, mainly because the pollutant adsorption is accompanied a slightly substrate reconstruction under covalent binding and the Au_{20} energy levels are shifted; this improvement in the acceptor character of the Au_{20} cluster in the Au−As mode is clear from the $\omega_{Au_{20}}$ value, which is up to 3.0 eV higher with respect to the isolated cluster, while the systems in the Au−O mode reaches an increase of up to 0.3 eV. Second, the $As(OH)_3$ molecule increases its acceptor character in all of the different adducts with respect to its isolated form, but this increase is less when $As(OH)_3$ is adsorbed in the Au−As mode. These effects cause $\Delta\mu$ and $\Delta\omega$ values to be larger in systems **I**, **III**, and **V**, and thus the larger electron transfer is expected in these cases, in good agreement with the results displayed in Table 1.

On the contrary, we observe that the HOMO−LUMO energy gap (HL_{gap}) (Figure 3) in all systems tends to decrease

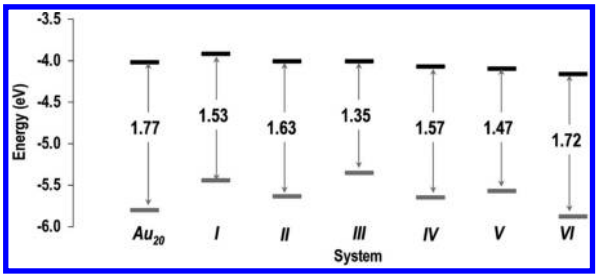

Figure 3. HOMO (gray) and LUMO (black) energy levels of systems **I**−**VI** and the tetrahedral Au_{20} cluster.

as the electron transfer increases; that is, the largest reactivity of the whole system (the lowest HL_{gap}) is reached with a relative strong interaction with the pollutant molecule, which is allowed in the Au−As mode. At this respect, the Au−As conformations show the lowest HL_{gap} of the order of 1.55 to 1.35 eV, while the Au−O modes have HL_{gap} on the order of 1.64 to 1.57 eV; in both cases, the lowest values are reached when Au^e serves as adsorption site. Note that the system **VI** shows a low change in the HL_{gap} compared with the Au_{20} cluster, which is consistent with a noncovalent interaction. These changes in the HL_{gap} are associated mainly with the destabilization of the HOMO of the Au_{20} cluster due to its hybridization with the HOMO of the pollutant, an effect that is pronounced with the strengthening of the metal−$As(OH)_3$ bond. In summary, the results indicate that the chemisorption of $As(OH)_3$ on the substrate results in a lower HL_{gap}, that is, an enhanced reactivity that is depending of the different adsorbent−adsorbate conformations. In this

DOI: 10.1021/acs.jpca.5b03832
J. Phys. Chem. A XXXX, XXX, XXX−XXX

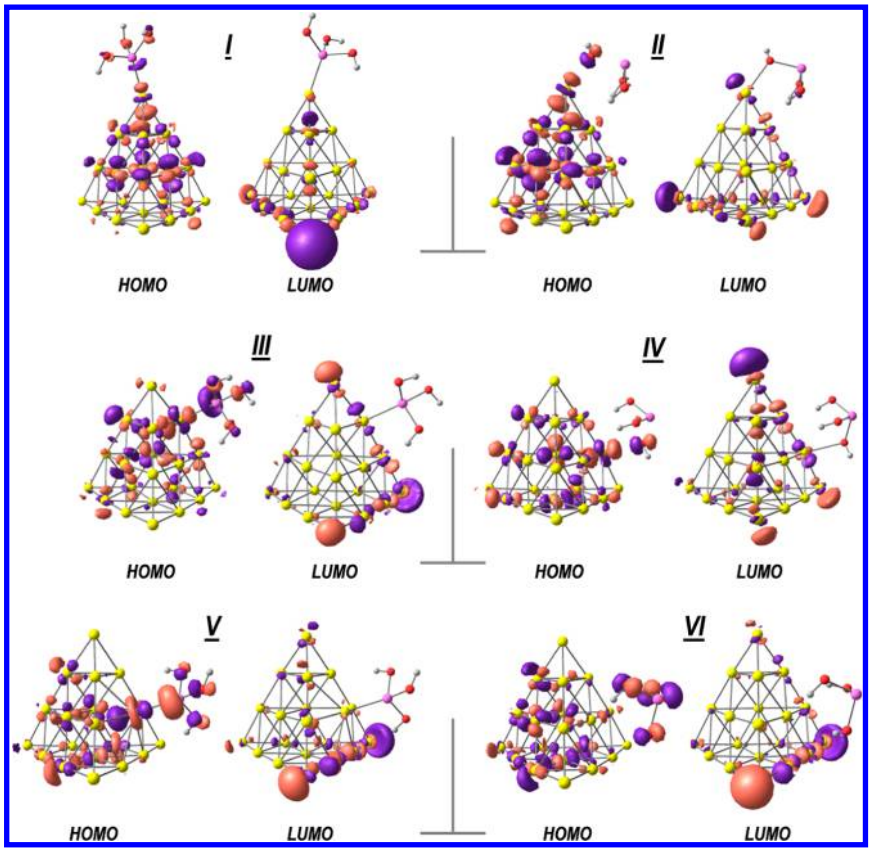

Figure 4. HOMO (H) and LUMO (L) surfaces of systems **I**–**VI**.

respect, we need to point out that in the case of graphitic-based electrodes, the As(III) interaction on graphitic surfaces is lowly stable in an aqueous environment (E_{ads} < 0.3 eV),[62] and thus the Au_{20}-embedded electrodes can serve as improved sensing platforms of As(III) due to the ability to bond the pollutant and to change both the electronic and conductive properties of the substrate.

The adsorbent–adsorbate interaction breaks the T_d symmetry of the Au_{20} cluster; then, the degeneracy of the HOMO and LUMO disappears. However, these molecular orbitals on the $Au_{20}\cdots As(OH)_3$ systems appear, still retaining the topology as in the isolated Au_{20} cluster (Figure 4). The latter indicates that the LUMO is mainly delocalized in the Au^v atoms without contribution from the $As(OH)_3$ molecule, which is in agreement with the low differences in the energy of the LUMO level between the systems **I**–**VI**; however, the HOMO is delocalized onto the Au^e and Au^i atoms, with contribution of the adsorbent site, in addition to contributions either from the arsenic or oxygen atoms according to whether the conformation is Au–As, Au–O and the type of adsorption site, which explains why the shifting in the HOMO energy is larger with respect to that of the LUMO level. In systems **I**–**II**, the HOMO is also composed of s orbitals of the adsorbent Au^v atom; while, for adsorption in Au^e (**III, IV**) and Au^i (**V**), the HOMO has contribution from the s–$d_{x^2-y^2}$ and d_{z^2} orbitals of the adsorbent atom, respectively. In addition, the s and p orbitals of arsenic contribute to HOMO in the Au–As and Au–O modes, respectively. Moreover, the MEP surfaces (Figure 5) indicate that the vacant adsorption sites keep their charge as in the isolated Au_{20} cluster: positive for Au^v, negative for Au^i, and almost neutral for Au^e. On the basis of these results, it can be expected that the vacant sites are able to a subsequent pollutant adsorption by combination of charge- and orbital-controlled interactions.

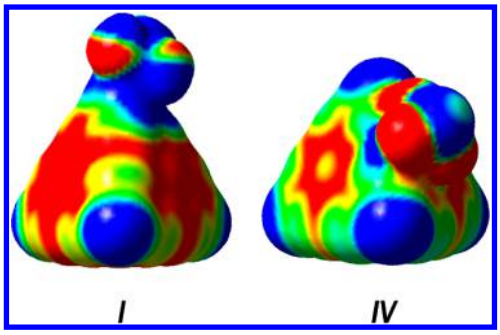

Figure 5. MEP surfaces of systems **I** and **IV**, selected as representatives for all $Au_{20}\cdots As(OH)_3$ systems. Sites with negative and positive charge excesses are characterized by red and blue color, respectively.

3.2. Effect of the Pt Doping: Adsorption onto $Au_{19}Pt$ Cluster. If increased adsorption energies are desirable, we can try doped gold nanostructures. The effect of dopant atoms on the chemical reactivity of gold has been extensively studied by computational chemists[64−67] and also demonstrated by experimentalists,[68−70] which have shown that transition metals enhance the chemical reactivity toward adsorption of different molecules like CO, O_2, and H_2O_2. To explore this alternative and effects of the dopant on the properties of the adsorbent–$As(OH)_3$ systems, we analyze the adsorption on the bimetallic $Au_{19}Pt$ cluster, which has been proposed with a high stability by means of the strong Au–Pt interaction.[14] Morrow and coworkers[71] have demonstrated that the Pt doping of gold nanostructures advantage the adsorption of molecules such as CO; in this case, the CO adsorption energy onto the Pt site is

DOI: 10.1021/acs.jpca.5b03832
J. Phys. Chem. A XXXX, XXX, XXX–XXX

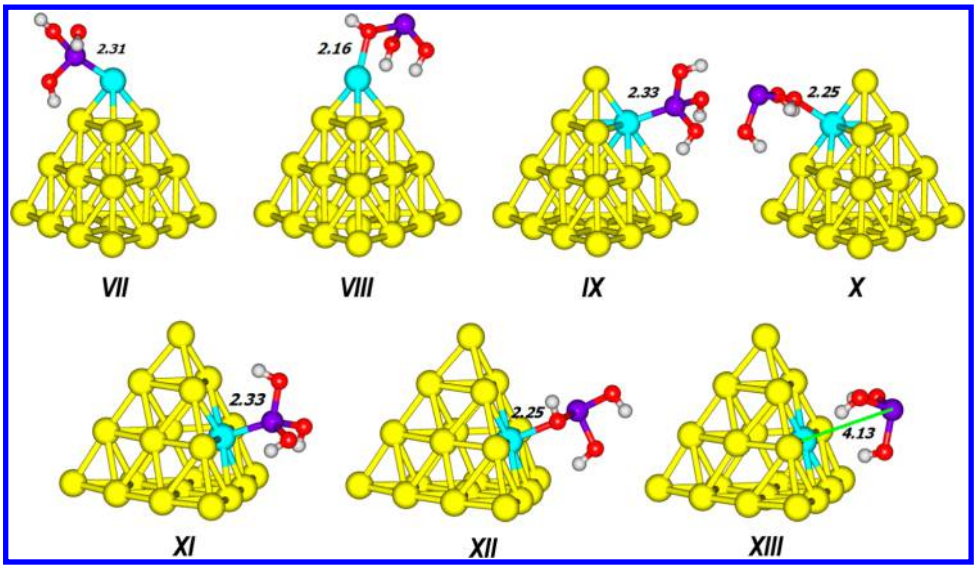

Figure 6. Optimized molecular structures of the $Au_{19}Pt\cdots As(OH)_3$ systems. Color code to atoms: white, hydrogen; red, oxygen; purple, arsenic; yellow, gold; sky-blue, platinum.

increased 1 eV with respect to the adsorption on the Au site.[71] Moreover, an enhanced reactivity and improved adsorption energies have been obtained for the adsorption of CO and O_2 onto the bimetallic $Au_{19}Pt$ and $Au_{12}Pt$ clusters.[52,72] Note that the experimental monodoping of gold nanostructures with platinum dopants and their improvement for catalytic activity has also been achieved by Qian and coworkers.[68]

The results for the $Au_{19}Pt\cdots As(OH)_3$ systems are summarized in Figure 6 and Table 3. As in the undoped case, arsenite can bind to $Au_{19}Pt$ by Pt−As (**VII**, **IX**, **XI**) or Pt−O (**VIII**, **X**, **XII**) bonds, with the bond lengths on the order of d_{Pt-As} = 2.31 to 2.33 and d_{Pt-O} = 2.16 to 2.25 Å, respectively (Figure 6). The pollutant physisorption onto the plane with the Pt^i atom (**XIII**) take place at d_{Pt-As} = 4.13 Å. The adsorption energies indicate that the metal-As mode (**VII**, **IX**, **XI**) is the most stable as in the Au_{20}−$As(OH)_3$ systems, but the adsorption energies are significantly increased to values on the order of 1.66 to 1.82 eV, as suggested from the shorter bond lengths. Moreover, the Pt−O mode also shows an increasing in the adsorption energies with respect to the Au_{20} cluster, but the improvement is depending on the adsorbent Pt type atom; for instance, for the Pt^v, Pt^e, or Pt^i adsorption sites, adsorption energies decrease as 1.34, 0.95, and 0.65 eV, respectively. Note that the values for adsorption energies are even higher, as obtained with minerals such as aluminum oxides,[73] which are on the order of 0.96 to 1.23 eV. Finally, the pollutant physisorption onto the adsorbent (system **XIII**) is found with only an increase in 0.07 eV with respect to the physisorption onto Au_{20}. It is important to note that the Pt−As bond has a covalent character due to the interaction between hybridized sp orbitals of both As and Pt atoms, where at least 76% of the bonding density is polarized toward the positively charged arsenic atom. The coordinative Pt−O bond appears as an interaction between the oxygen lone pair and an antibonding 6p orbital of the Pt atom, which result in a decrease in the bonding stability, as noted from the adsorption energies; moreover, interaction with oxygen atom is enhanced by interaction with the half-filled $5d_{z^2}$ orbital of platinum and an electrostatic interaction between hydrogen atoms directed toward the neighboring Au^e atoms in the adsorbent.

Table 3. Selected Atomic and Fragment Charges of the $Au_{19}Pt\cdots As(OH)_3$ Systems

		charge of the adsorption site Pt^x				
system	E_{ads}	before adsorption	after adsorption	ΔQ_{Pt}	$Q_{As(OH)_3}$	Q_{As}
VII	1.80	−0.05	−0.42	−0.36	0.51	1.82
VIII	1.34	−0.05	−0.17	−0.11	0.28	1.59
IX	1.82	−0.35	−0.94	−0.59	0.64	1.92
X	0.95	−0.35	−0.47	−0.12	0.31	1.61
XI	1.66	−0.69	−1.28	−0.59	0.78	1.99
XII	0.65	−0.69	−0.71	−0.02	0.42	1.68
XIII	0.61	−0.69	−1.00	−0.31	0.21	1.59

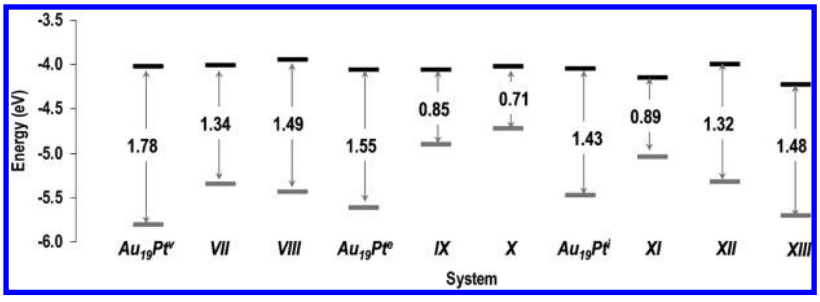

Figure 7. SOMO (gray) and LUMO (black) energy levels of systems **VII**−**XIII** and the tetrahedral $Au_{19}Pt$ clusters.

DOI: 10.1021/acs.jpca.5b03832
J. Phys. Chem. A XXXX, XXX, XXX−XXX

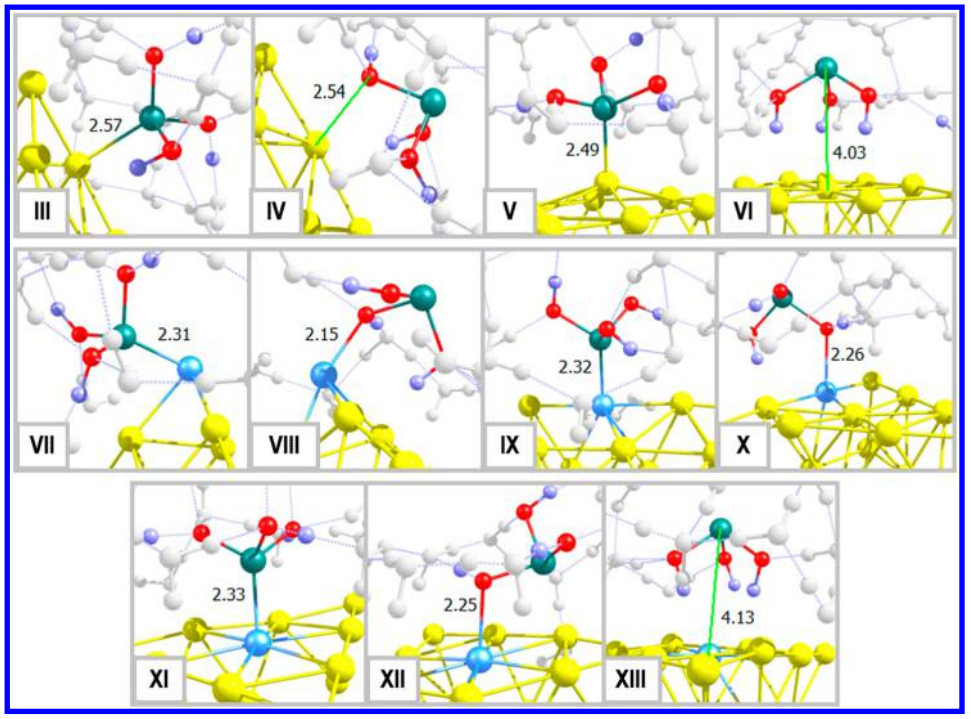

Figure 8. Optimized structures of $Au_{20}\cdots As(OH)_3$ (**III**–**VI**) and $Au_{19}Pt\cdots As(OH)_3$ (**VII**–**XIII**) systems in a explicit solvent environment. H_2O molecules are depicted in white with pointed hydrogen bonds.

In addition, we observed a high electron transfer in the $As(OH)_3 \rightarrow Au_{19}Pt$ direction (up to 0.78*e*) taking place in the Pt–As mode, in agreement with its higher stability compared with the Pt–O mode (which reaches a charge transfer of up to 0.12*e*, mainly because the bond in this case is coordinative). At first glance, the enhanced $As(OH)_3$ interaction in the $Au_{19}Pt$ clusters can be explained in terms of an increased charge transfer and orbital interaction, besides the Pt–As bond has an important electrostatic contribution as noted from the charges of the Pt and As atoms after interaction, which shows a high change of up to 0.59|*e*|, explaining the high stability of this bond compared with the Au–As bonding.

Moreover, the chemical interaction with the pollutant causes a decrease in the HL_{gap} for all of the conformations (except the physisorbed case) (Figure 7), indicating an increased reactivity in all of the adsorbents after the pollutant is chemisorbed, even with lower HL_{gap} with respect to the interaction onto Au_{20}, suggesting an increased performance to sensing. From Figure 7, it is noted that the HL_{gap} in the $Au_{19}Pt$ cluster is depending on the doping site, as suggested by Mondal and coworkers, which is associated with their related stabilities.[52] The $Au_{19}Pt^{v}$ cluster has a similar reactivity as Au_{20} with an HL_{gap} = 1.78 eV, while $Au_{19}Pt^{e}$ and $Au_{19}Pt^{i}$ show HL_{gap} values of 1.55 and 1.43 eV, respectively, indicating their enhanced reactivities. (Note that HOMO in the $Au_{19}Pt$ cluster specifically is the SOMO due to its open-shell structure.)

Finally, these results show that the ability of the Au_{20} cluster for the pollutant capture and sensing is improved by the doping with platinum, even when the dopant concentration is <5%. In this respect, it is important to point out that the desorption energy of the pollutant is higher from the $Au_{19}Pt$ than from the Au_{20} cluster, which could decrease the recovery and cycles of use of the modified electrodes. Although the later request of experimental measures of the electrode stability, it is well known that trivalent arsenic compounds are straightforward to remove from substrates by means of alkaline solutions (pH >12).[3]

3.3. Solvent Effects. The high mobility of As(III) from several substrates in aqueous solutions, which reduces the ability of detection and removal, or the possibility of catalytic processes to form As(V) is known.[8] In this respect, the calculations of adsorption energies give good results in the context that they are stable, but it is expected that the solvation energy affects the adsorption strength in an aqueous environment. Adsorption energies were estimated for all systems from three implicit continuum solvent methods as SMD,[74] IEF-PCM,[75] and C-PCM,[76,77] observing nonregular variations between all of the methodologies to obtain the adsorption energies, which shows variations in the range of up to ±0.2 eV, suggesting that all of the conformations are stable in a solvent media; however, to account correctly for the effects of the solvent molecules in the structural properties of the cluster–pollutant systems, the stability of the metal-As and metal-O bonding by surrounding the pollutant with 12 H_2O molecules and optimizing the entire system was analyzed. From several optimizations, the most stable conformations are displayed in Figure 8.

As can be seen in Figure 8, the Au^{v}–pollutant bond turns unstable in an explicit solvent environment, and solvent molecules cause the diffusion of the $As(OH)_3$ molecule from the adsorption site toward the Au^{e} or Au^{i} atoms to be adsorbed either the Au–As or Au–O mode. The latter can be explained because the water molecules can bond to the Au^{v} atom, while the pollutant has a larger area exposed to the solvent molecules in the vertices compared with respect to adsorption in the edges and inner cluster sides, favoring the solvation by the H_2O molecules. On the contrary, the interaction modes depicted by systems **III**–**VI** are even stable in a water environment, with a change in the bond length for the metal–pollutant bond of up to ±0.03 Å. A similar analysis was performed for the $Au_{19}Pt\cdots$

DOI: 10.1021/acs.jpca.5b03832
J. Phys. Chem. A XXXX, XXX, XXX–XXX

$As(OH)_3$ systems (**VII**−**XIII**); in all of the conformations, both the Pt−As and Pt−O modes were not significantly affected by the solvent. Indeed, the water molecules tend to form a cluster surrounding the pollutant molecule, but the high adsorption energies of these systems allow us to retain the metal−pollutant binding, which shows low changes in the bond lengths of up to ±0.01 Å. It is worth noting that the OH group of the pollutant slightly elongates its bond length, suggesting that the hydrogen turns labile in the presence of the solvent; it is expected that the arsenite in its $As(OH)_{3-n}O^{-n}$ form still remains adsorbed and stabilized onto the doped adsorbents due to the strong chemical bonding.

4. CONCLUSIONS

In summary, it was determined that arsenic(III) under neutral conditions is capable to interact onto the tetrahedral Au_{20} cluster either by their vertex, edge, or inner gold atoms. The interactions were observed to have a covalent character by forming of metal−arsenic or metal−oxygen bonding, with adsorption energies on the range of 0.5 to 0.8 eV, even with a stable physisorption onto the tetrahedral plane; however, in an aqueous media, the Au^{vertex}−pollutant interaction was determined to be disadvantageous, while interaction with inner and edge gold atoms remains stable. Moreover, a subsequent adsorption of pollutants would be possible because the available adsorption sites keep the reactivity toward both orbital and charge-controlled interactions. The substituent effect of the Pt doping into the properties of the adsorbent−adsorbate systems was evaluated by using the $Au_{19}Pt$ cluster as support. It was found that the dopant atom increases both the metal−pollutant interaction and the stability in a water media for all interaction modes; in these cases, the adsorption energies are in the range 1.8 to 0.6 eV. All of the studied interactions are accompanied by changes in the reactivity, electron transfer, and a decrease in the HOMO−LUMO energy gap with respect to the isolated substrate, offering an alternative to improve the detection of the pollutant. By this work, we can get insights into the adsorption and detection of trivalent arsenic traces from polluted waters by means of embedded electrodes with gold nanostructures and gold nanoparticles.

■ ASSOCIATED CONTENT

Supporting Information

Reliability of the selected method, discussion about geometry and the HOMO−LUMO surfaces of the $Au_{19}Pt$−$As(OH)_3$ systems. The Supporting Information is available free of charge on the ACS Publications website at DOI: 10.1021/acs.jpca.5b03832.

■ AUTHOR INFORMATION

Corresponding Author

*E-mail: dcortesr@uc.cl.

Notes

The authors declare no competing financial interest.

■ ACKNOWLEDGMENTS

This work was supported by the project: FONDECYT/Postdoctorado no. 3140314, FONDECYT 1130072, and ICM grant no. 120082. D.C-A. acknowledges N. Villegas for comments.

■ REFERENCES

(1) Mondal, P.; Majumder, C.; Mohanty, B. Laboratory Based Approaches for Arsenic Remediation from Contaminated Water: Recent Developments. *J. Hazard. Mater.* **2006**, *137*, 464−479.
(2) Bundschuh, J.; Bhattacharya, P.; Sracek, O.; Mellano, M. F.; Ramirez, A. E.; Storniolo, A. d. R.; Martin, R. A.; Cortes, J.; Litter, M. I.; Jean, J.-S. Arsenic Removal from Groundwater of the Chaco-Pampean Plain (Argentina) Using Natural Geological Materials as Adsorbents. *J. Environ. Sci. Health, Part A* **2011**, *46*, 1297−1310.
(3) Singh, R.; Singh, S.; Parihar, P.; Singh, V. P.; Prasad, S. M. Arsenic Contamination, Consequences and Remediation Techniques: A Review. *Ecotoxicol. Environ. Saf.* **2015**, *112*, 247−270.
(4) Anderson, L. C.; Bruland, K. W. Biogeochemistry of Arsenic in Natural Waters: The Importance of Methylated Species. *Environ. Sci. Technol.* **1991**, *25*, 420−427.
(5) Andreae, M. O. Determination of Arsenic Species in Natural Waters. *Anal. Chem.* **1977**, *49*, 820−823.
(6) Braman, R. S.; Foreback, C. C. Methylated Forms of Arsenic in the Environment. *Science* **1973**, *182*, 1247−1249.
(7) Liu, Z.-G.; Huang, X.-J. Voltammetric Determination of Inorganic Arsenic. *TrAC, Trends Anal. Chem.* **2014**, *60*, 25−35.
(8) Ferguson, J. F.; Gavis, J. A Review of the Arsenic Cycle in Natural Waters. *Water Res.* **1972**, *6*, 1259−1274.
(9) Domínguez-González, R.; Varela, L. G.; Bermejo-Barrera, P. Functionalized Gold Nanoparticles for the Detection of Arsenic in Water. *Talanta* **2014**, *118*, 262−269.
(10) Liu, Y.; Huang, Z.; Xie, Q.; Sun, L.; Gu, T.; Li, Z.; Bu, L.; Yao, S.; Tu, X.; Luo, X. Electrodeposition of Electroreduced Graphene Oxide-Au Nanoparticles Composite Film at Glassy Carbon Electrode for Anodic Stripping Voltammetric Analysis of Trace Arsenic (III). *Sens. Actuators, B* **2013**, *188*, 894−901.
(11) Thomas, P.; Sniatecki, K. Determination of Trace Amounts of Arsenic Species in Natural Waters by High-Performance Liquid Chromatography−Inductively Coupled Plasma Mass Spectrometry. *J. Anal. At. Spectrom.* **1995**, *10*, 615−618.
(12) Arslan, Y.; Yildirim, E.; Gholami, M.; Bakirdere, S. Lower Limits of Detection in Speciation Analysis by Coupling High-Performance Liquid Chromatography and Chemical-Vapor Generation. *TrAC, Trends Anal. Chem.* **2011**, *30*, 569−585.
(13) Colon, M.; Hidalgo, M.; Iglesias, M. Arsenic Determination by ICP-QMS with Octopole Collision/Reaction Cell. Overcome of Matrix Effects under Vented and Pressurized Cell Conditions. *Talanta* **2011**, *85*, 1941−1947.
(14) Tavakkoli, N.; Habibollahi, S.; Amini Tehrani, S. Modified Activated Carbon as Solid Phase Extraction Adsorbent for the Preconcentration and Determination of Trace as (III) in Environmental Samples by Graphite Furnace Atomic Absorption Spectrometry. *Chin. J. Chem.* **2012**, *30*, 665−669.
(15) Cacho, F.; Lauko, L.; Manova, A.; Beinrohr, E. On-Line Electrochemical Pre-Concentration of Arsenic on a Gold Coated Porous Carbon Electrode for Graphite Furnace Atomic Absorption Spectrometry. *J. Anal. At. Spectrom.* **2012**, *27*, 695−699.
(16) Williams, D. G.; Johnson, D. C. Pulsed Voltammetric Detection of Arsenic (III) at Platinum Electrodes in Acidic Media. *Anal. Chem.* **1992**, *64*, 1785−1789.
(17) Li, H.; Smart, R. B. Determination of Sub-Nanomolar Concentration of Arsenic (III) in Natural Waters by Square Wave Cathodic Stripping Voltammetry. *Anal. Chim. Acta* **1996**, *325*, 25−32.
(18) Adeloju, S.; Young, T.; Jagner, D.; Batley, G. Constant Current Cathodic Stripping Potentiometric Determination of Arsenic on a Mercury Film Electrode in the Presence of Copper Ions. *Anal. Chim. Acta* **1999**, *381*, 207−213.
(19) Prakash, R.; Srivastava, R.; Seth, P. Direct Estimation of Total Arsenic Using a Novel Metal Side Disk Rotating Electrode. *Electroanalysis* **2003**, *15*, 1410−1414.
(20) Wei, Z.; Somasundaran, P. Cyclic Voltammetric Study of Arsenic Reduction and Oxidation in Hydrochloric Acid Using a Pt Rde. *J. Appl. Electrochem.* **2004**, *34*, 241−244.

DOI: 10.1021/acs.jpca.5b03832
J. Phys. Chem. A XXXX, XXX, XXX−XXX

(21) Hossain, M.; Islam, M.; Ferdousi, S.; Okajima, T.; Ohsaka, T. Anodic Stripping Voltammetric Detection of Arsenic (III) at Gold Nanoparticle-Modified Glassy Carbon Electrodes Prepared by Electrodeposition in the Presence of Various Additives. *Electroanalysis* **2008**, *20*, 2435−2441.
(22) Du, Y.; Zhao, W.; Xu, J.-J.; Chen, H.-Y. Electrochemical Determination of Arsenite in Neutral Media on Reusable Gold Nanostructured Films. *Talanta* **2009**, *79*, 243−248.
(23) Huang, J.-F.; Chen, H.-H. Gold-Nanoparticle-Embedded Nafion Composite Modified on Glassy Carbon Electrode for Highly Selective Detection of Arsenic (III). *Talanta* **2013**, *116*, 852−859.
(24) Gu, T.; Bu, L.; Huang, Z.; Liu, Y.; Tang, Z.; Liu, Y.; Huang, S.; Xie, Q.; Yao, S.; Tu, X.; et al. Dual-Signal Anodic Stripping Voltammetric Determination of Trace Arsenic(III) at a Glassy Carbon Electrode Modified with Internal-Electrolysis Deposited Gold Nanoparticles. *Electrochem. Commun.* **2013**, *33*, 43−46.
(25) Ramesha, G.; Sampath, S. In-Situ Formation of Graphene−Lead Oxide Composite and Its Use in Trace Arsenic Detection. *Sens. Actuators, B* **2011**, *160*, 306−311.
(26) Profumo, A.; Fagnoni, M.; Merli, D.; Quartarone, E.; Protti, S.; Dondi, D.; Albini, A. Multiwalled Carbon Nanotube Chemically Modified Gold Electrode for Inorganic as Speciation and Bi (III) Determination. *Anal. Chem.* **2006**, *78*, 4194−4199.
(27) Xiao, L.; Wildgoose, G. G.; Compton, R. G. Sensitive Electrochemical Detection of Arsenic (III) Using Gold Nanoparticle Modified Carbon Nanotubes Via Anodic Stripping Voltammetry. *Anal. Chim. Acta* **2008**, *620*, 44−49.
(28) Xu, H.; Zeng, L.; Xing, S.; Xian, Y.; Jin, L. Microwave-Irradiated Synthesized Platinum Nanoparticles/Carbon Nanotubes for Oxidative Determination of Trace Arsenic (III). *Electrochem. Commun.* **2008**, *10*, 551−554.
(29) Shin, S.-H.; Hong, H.-G. Anodic Stripping Voltammetric Detection of Arsenic (III) at Platinum-Iron (III) Nanoparticle Modified Carbon Nanotube on Glassy Carbon Electrode. *Bull. Korean Chem. Soc.* **2010**, *31*, 3077−3083.
(30) Lan, Y.; Luo, H.; Ren, X.; Wang, Y.; Wang, L. Glassy Carbon Electrode Modified with Citrate Stabilized Gold Nanoparticles for Sensitive Arsenic (III) Detection. *Anal. Lett.* **2012**, *45*, 1184−1196.
(31) Thotiyl, M. O.; Basit, H.; Sánchez, J. A.; Goyer, C.; Coche-Guerente, L.; Dumy, P.; Sampath, S.; Labbé, P.; Moutet, J.-C. Multilayer Assemblies of Polyelectrolyte−Gold Nanoparticles for the Electrocatalytic Oxidation and Detection of Arsenic (III). *J. Colloid Interface Sci.* **2012**, *383*, 130−139.
(32) Mardegan, A.; Scopece, P.; Lamberti, F.; Meneghetti, M.; Moretto, L.; Ugo, P. Electroanalysis of Trace Inorganic Arsenic with Gold Nanoelectrode Ensembles. *Electroanalysis* **2012**, *24*, 798−806.
(33) Dai, X.; Wildgoose, G. G.; Salter, C.; Crossley, A.; Compton, R. G. Electroanalysis Using Macro-, Micro-, and Nanochemical Architectures on Electrode Surfaces. Bulk Surface Modification of Glassy Carbon Microspheres with Gold Nanoparticles and Their Electrical Wiring Using Carbon Nanotubes. *Anal. Chem.* **2006**, *78*, 6102−6108.
(34) Häkkinen, H. Atomic and Electronic Structure of Gold Clusters: Understanding Flakes, Cages and Superatoms from Simple Concepts. *Chem. Soc. Rev.* **2008**, *37*, 1847−1859.
(35) Nambiar, S. R.; Prathish, K. P.; Karthik, G.; Rao, T. P. Hybrid Gold Atomic Cluster−Cobalt Oxide Scaffolds for Dual Tandem Electrocatalytic Sensing of Cysteine. *Biosens. Bioelectron.* **2011**, *26*, 3920−3926.
(36) Boyen, H.-G.; Kästle, G.; Weigl, F.; Koslowski, B.; Dietrich, C.; Ziemann, P.; Spatz, J.; Riethmüller, S.; Hartmann, C.; Möller, M. Oxidation-Resistant Gold-55 Clusters. *Science* **2002**, *297*, 1533−1536.
(37) Aikens, C. M.; Schatz, G. C. TDDFT Studies of Absorption and SERs Spectra of Pyridine Interacting with $_{>Au_{20}}$. *J. Phys. Chem. A* **2006**, *110*, 13317−13324.
(38) Haruta, M.; Yamada, N.; Kobayashi, T.; Iijima, S. Gold Catalysts Prepared by Coprecipitation for Low-Temperature Oxidation of Hydrogen and of Carbon Monoxide. *J. Catal.* **1989**, *115*, 301−309.
(39) Li, J.; Li, X.; Zhai, H.-J.; Wang, L.-S. Au_{20}: A Tetrahedral Cluster. *Science* **2003**, *299*, 864−867.
(40) Wang, J.; Wang, G.; Zhao, J. Structures and Electronic Properties of Cu_{20}, Ag_{20}, and Au_{20} Clusters with Density Functional Method. *Chem. Phys. Lett.* **2003**, *380*, 716−720.
(41) King, R. B.; Chen, Z.; Schleyer, P. R. Structure and Bonding in the Omnicapped Truncated Tetrahedral Au_{20} Cluster: Analogies between Gold and Carbon Cluster Chemistry. *Inorg. Chem.* **2004**, *43*, 4564−4566.
(42) Fernández, E. M.; Soler, J. M.; Garzón, I. L.; Balbás, L. C. Trends in the Structure and Bonding of Noble Metal Clusters. *Phys. Rev. B* **2004**, *70*, 165403.
(43) Zhang, C.; Yoon, B.; Landman, U. Predicted Oxidation of Co Catalyzed by Au Nanoclusters on a Thin Defect-Free MgO Film Supported on a Mo(100) Surface. *J. Am. Chem. Soc.* **2007**, *129*, 2228−2229.
(44) Perdew, J. P.; Burke, K.; Ernzerhof, M. Generalized Gradient Approximation Made Simple. *Phys. Rev. Lett.* **1996**, *77*, 3865.
(45) Dill, J. D.; Pople, J. A. Self-Consistent Molecular Orbital Methods. XV. Extended Gaussian-Type Basis Sets for Lithium, Beryllium, and Boron. *J. Chem. Phys.* **1975**, *62*, 2921−2923.
(46) Francl, M. M.; Pietro, W. J.; Hehre, W. J.; Binkley, J. S.; Gordon, M. S.; DeFrees, D. J.; Pople, J. A. Self-Consistent Molecular Orbital Methods. Xxiii. A Polarization-Type Basis Set for Second-Row Elements. *J. Chem. Phys.* **1982**, *77*, 3654−3665.
(47) Hay, P. J.; Wadt, W. R. Ab Initio Effective Core Potentials for Molecular Calculations. Potentials for K to Au Including the Outermost Core Orbitals. *J. Chem. Phys.* **1985**, *82*, 299−310.
(48) Roy, L. E.; Hay, P. J.; Martin, R. L. Revised Basis Sets for the Lanl Effective Core Potentials. *J. Chem. Theory Comput.* **2008**, *4*, 1029−1031.
(49) Ehlers, A.; Böhme, M.; Dapprich, S.; Gobbi, A.; Höllwarth, A.; Jonas, V.; Köhler, K.; Stegmann, R.; Veldkamp, A.; Frenking, G. A Set of F-Polarization Functions for Pseudo-Potential Basis Sets of the Transition Metals Sc-Cu, Y-Ag and La-Au. *Chem. Phys. Lett.* **1993**, *208*, 111−114.
(50) Schuchardt, K. L.; Didier, B. T.; Elsethagen, T.; Sun, L.; Gurumoorthi, V.; Chase, J.; Li, J.; Windus, T. L. Basis Set Exchange: A Community Database for Computational Sciences. *J. Chem. Inf. Model.* **2007**, *47*, 1045−1052.
(51) Feller, D. The Role of Databases in Support of Computational Chemistry Calculations. *J. Comput. Chem.* **1996**, *17*, 1571−1586.
(52) Mondal, K.; Banerjee, A.; Ghanty, T. K. Structural and Chemical Properties of Subnanometer-Sized Bimetallic $Au_{19}Pt$ Cluster. *J. Phys. Chem. C* **2014**, *118*, 11935−11945.
(53) Grimme, S.; Ehrlich, S.; Goerigk, L. Effect of the Damping Function in Dispersion Corrected Density Functional Theory. *J. Comput. Chem.* **2011**, *32*, 1456−1465.
(54) Grimme, S.; Antony, J.; Ehrlich, S.; Krieg, H. A Consistent and Accurate Ab Initio Parametrization of Density Functional Dispersion Correction (DFT-D) for the 94 Elements H-Pu. *J. Chem. Phys.* **2010**, *132*, 154104.
(55) Boys, S. F.; Bernardi, F. d. The Calculation of Small Molecular Interactions by the Differences of Separate Total Energies. Some Procedures with Reduced Errors. *Mol. Phys.* **1970**, *19*, 553−566.
(56) Frisch, M. J.; Trucks, G. W.; Schlegel, H. B.; Scuseria, G. E.; Robb, M. A.; Cheeseman, J. R.; Scalmani, G.; Barone, V.; Mennucci, B.; Petersson, G. A.; et al. *Gaussian 09*, revision B.01; Gaussian, Inc.: Wallingford, CT, 2009.
(57) Kryachko, E.; Remacle, F. The Magic Gold Cluster Au_{20}. *Int. J. Quantum Chem.* **2007**, *107*, 2922−2934.
(58) Sevillano, P.; Fuhr, O.; Kattannek, M.; Nava, P.; Hampe, O.; Lebedkin, S.; Ahlrichs, R.; Fenske, D.; Kappes, M. M. The Phosphine-Stabilized Gold−Arsenic Clusters $[Au_{19}(Asnpr_8(Dppe)_6]C_{l3}$, $[Au_{10}(Asnpr)_4(Dppe)_4]C_{l2}$,$[Au_{17}(Asnpr)_6(As_2npr_2)(Dppm)_6]C_{l3}$, and$[Au_{10}(Asph)_4(Dppe)_4]C_{l2}$: Synthesis, Characterization, and DFT Calculations. *Angew. Chem., Int. Ed.* **2006**, *45*, 3702−3708.
(59) Gimeno, M. C.; Laguna, A.; Three-and Four-Coordinate. Gold (I) Complexes. *Chem. Rev.* **1997**, *97*, 511−522.

DOI: 10.1021/acs.jpca.5b03832
J. Phys. Chem. A XXXX, XXX, XXX−XXX

(60) Chaki, N. K.; Mandal, S.; Reber, A. C.; Qian, M.; Saavedra, H. M.; Weiss, P. S.; Khanna, S. N.; Sen, A. Controlling Band Gap Energies in Cluster-Assembled Ionic Solids through Internal Electric Fields. *ACS Nano* **2010**, *4*, 5813−5818.
(61) Griffe, B.; Brito, J. L.; Sierraalta, A. Theoretical Study of Co Adsorption and Oxidation on Au_{3-5} Clusters Supported on Silico-Aluminophospates. *Comput. Theor. Chem.* **2014**, *1042*, 69−83.
(62) Cortés-Arriagada, D.; Toro-Labbé, A. Improving as (III) Adsorption on Graphene Based Surfaces: Impact of Chemical Doping. *Phys. Chem. Chem. Phys.* **2015**, *17*, 12056−12064.
(63) Geerlings, P.; De Proft, F.; Langenaeker, W. Conceptual Density Functional Theory. *Chem. Rev.* **2003**, *103*, 1793−1874.
(64) Molina, L. M.; Hammer, B. The Activity of the Tetrahedral Au_{20} Cluster: Charging and Impurity Effects. *J. Catal.* **2005**, *233*, 399−404.
(65) Jena, N. K.; Chandrakumar, K.; Ghosh, S. K. Theoretical Investigation on the Structure and Electronic Properties of Hydrogen- and Alkali-Metal-Doped Gold Clusters and Their Interaction with Co: Enhanced Reactivity of Hydrogen-Doped Gold Clusters. *J. Phys. Chem. C* **2009**, *113*, 17885−17892.
(66) Nhat, P. V.; Tai, T. B.; Nguyen, M. T. Theoretical Study of Au_nV-Co, N=1−14: The Dopant Vanadium Enhances Co Adsorption on Gold Clusters. *J. Chem. Phys.* **2012**, *137*, 164312.
(67) Beletskaya, A. V.; Pichugina, D. A.; Shestakov, A. F.; Kuz'menko, N. E. Formation of H_2O_2 on Au_{20} and Au_{19}Pd Clusters: Understanding the Structure Effect on the Atomic Level. *J. Phys. Chem. A* **2013**, *117*, 6817−6826.
(68) Qian, H.; Jiang, D.-e.; Li, G.; Gayathri, C.; Das, A.; Gil, R. R.; Jin, R. Monoplatinum Doping of Gold Nanoclusters and Catalytic Application. *J. Am. Chem. Soc.* **2012**, *134*, 16159−16162.
(69) Le, H. T.; Lang, S. M.; De Haeck, J.; Lievens, P.; Janssens, E. Carbon Monoxide Adsorption on Neutral and Cationic Vanadium Doped Gold Clusters. *Phys. Chem. Chem. Phys.* **2012**, *14*, 9350−9358.
(70) De Haeck, J.; Veldeman, N.; Claes, P.; Janssens, E.; Andersson, M.; Lievens, P. Carbon Monoxide Adsorption on Silver Doped Gold Clusters. *J. Phys. Chem. A* **2011**, *115*, 2103−2109.
(71) Morrow, B. H.; Resasco, D. E.; Striolo, A.; Nardelli, M. B. Co Adsorption on Noble Metal Clusters: Local Environment Effects. *J. Phys. Chem. C* **2011**, *115*, 5637−5647.
(72) Liao, X.; Kuang, X. A Density Functional Theory Study on the Geometrical Structure and Chemical Reactivity of Binary Au_{12}Pt Cluster. *Eur. Phys. J. Plus* **2015**, *130*, 1−10.
(73) Oliveira, A. F.; Ladeira, A. C. Q.; Ciminelli, V. S. T.; Heine, T.; Duarte, H. A. Structural Model of Arsenic(III) Adsorbed on Gibbsite Based on DFT Calculations. *J. Mol. Struct.: THEOCHEM* **2006**, *762*, 17−23.
(74) Marenich, A. V.; Cramer, C. J.; Truhlar, D. G. Universal Solvation Model Based on Solute Electron Density and on a Continuum Model of the Solvent Defined by the Bulk Dielectric Constant and Atomic Surface Tensions. *J. Phys. Chem. B* **2009**, *113*, 6378−6396.
(75) Tomasi, J.; Mennucci, B.; Cances, E. The IEF Version of the PCM Solvation Method: An Overview of a New Method Addressed to Study Molecular Solutes at the QM Ab Initio Level. *J. Mol. Struct.: THEOCHEM* **1999**, *464*, 211−226.
(76) Barone, V.; Cossi, M. Quantum Calculation of Molecular Energies and Energy Gradients in Solution by a Conductor Solvent Model. *J. Phys. Chem. A* **1998**, *102*, 1995−2001.
(77) Cossi, M.; Rega, N.; Scalmani, G.; Barone, V. Energies, Structures, and Electronic Properties of Molecules in Solution with the C-PCM Solvation Model. *J. Comput. Chem.* **2003**, *24*, 669−681.

DOI: 10.1021/acs.jpca.5b03832
J. Phys. Chem. A XXXX, XXX, XXX−XXX